Draft version May 1, 2013
Preprint typeset using LaTeX style emulateapj v. 5/2/11

THE STELLAR INITIAL MASS FUNCTION OF ULTRA-FAINT DWARF GALAXIES:[1] EVIDENCE FOR IMF VARIATIONS WITH GALACTIC ENVIRONMENT

Marla Geha[2], Thomas M. Brown[3], Jason Tumlinson[3], Jason S. Kalirai[3], Joshua D. Simon[8], Evan N. Kirby[4,5], Don A. VandenBerg[6], Ricardo R. Muñoz[7], Roberto J. Avila[3], Puragra Guhathakurta[9], Henry C. Ferguson[3]

Draft version May 1, 2013

ABSTRACT

We present constraints on the stellar initial mass function (IMF) in two ultra-faint dwarf (UFD) galaxies, Hercules and Leo IV, based on deep *Hubble Space Telescope (HST)* Advanced Camera for Surveys (ACS) imaging. The Hercules and Leo IV galaxies are extremely low luminosity ($M_V = -6.2$, -5.5), metal-poor ($\langle$[Fe/H]$\rangle = -2.4$, -2.5) systems that have old stellar populations (> 11 Gyr). Because they have long relaxation times, we can directly measure the low-mass stellar IMF by counting stars below the main-sequence turnoff without correcting for dynamical evolution. Over the stellar mass range probed by our data, $0.52-0.77\,M_\odot$, the IMF is best fit by a power-law slope of $\alpha = 1.2^{+0.4}_{-0.5}$ for Hercules and $\alpha = 1.3 \pm 0.8$ for Leo IV. For Hercules, the IMF slope is more shallow than a Salpeter IMF ($\alpha = 2.35$) at the 5.8-σ level, and a Kroupa IMF ($\alpha = 2.3$ above $0.5\,M_\odot$) sat 5.4-σ level. We simultaneously fit for the binary fraction, finding $f_{\rm binary} = 0.47^{+0.16}_{-0.14}$ for Hercules, and $0.47^{+0.37}_{-0.17}$ for Leo IV. The UFD binary fractions are consistent with that inferred for Milky Way stars in the same mass range, despite very different metallicities. In contrast, the IMF slopes in the UFDs are shallower than other galactic environments. In the mass range 0.5 – 0.8 $M_\odot$, we see a trend across the handful of galaxies with directly measured IMFs such that the power-law slopes become shallower (more bottom-light) with decreasing galactic velocity dispersion and metallicity. This trend is qualitatively consistent with results in elliptical galaxies inferred via indirect methods and is direct evidence for IMF variations with galactic environment.

Subject headings: Local Group galaxies: dwarf galaxies: photometry galaxies: evolution galaxies: formation galaxies: stellar content

1. INTRODUCTION

The stellar initial mass function (IMF) parameterizes the relative number of stars formed in a single age population as a function of stellar mass. The IMF is fundamental to all calculations of star formation rates and galaxy stellar masses (for reviews see Bastian et al. 2010; Kroupa et al. 2011). The classic Salpeter (1955) IMF is a single power law with slope $\alpha = 2.35$ ($dN/dm \propto m^{-\alpha}$, where N is the number of stars of mass m). Salpeter's original IMF was based on stars down to $0.4\,M_\odot$, and modern Milky Way studies indicate a break in the IMF slope below this mass scale. Kroupa (2002) parameterized the Milky Way IMF as a broken power law, with $\alpha = 2.3$ above $0.5\,M_\odot$ and a shallower $\alpha = 1.3$ slope below this mass. Chabrier (2003, 2005) parameterized the IMF below $1\,M_\odot$ as a log-normal distribution with a characteristic mass $m_c \sim 0.2\,M_\odot$.

One may expect that the low mass IMF should depend on the physical properties of the stellar birth cloud such as the gas density, metallicity, or turbulent velocity (e.g.,; Larson 2005; Bate 2009; Myers et al. 2011; Marks et al. 2012; Hopkins 2012), however, IMF observations are largely invariant within the Milky Way (Bochanski et al. 2010; Covey et al. 2008). Recent indirect studies suggest that the low mass IMF slope does vary outside the Milky Way and may be a function of the global galactic potential: studies of integrated line strengths, kinematics and gravitational lensing studies of elliptical galaxies appear to favor IMFs that become increasingly bottom-heavy (with IMF slopes similar to or steeper than Salpeter) toward higher galaxy masses (Treu et al. 2010; van Dokkum & Conroy 2011; Cappellari et al. 2012a; Dutton et al. 2012; Conroy & van Dokkum 2012).

The ultra-faint dwarf (UFD) galaxies are a recent class of diffuse Galactic satellites discovered in Sloan Digital Sky Survey (SDSS) data (e.g., Willman et al. 2005; Belokurov et al. 2007). The UFDs are the least luminous ($-8 < M_V < -1.5$; Martin et al. 2008; Muñoz et al. 2010) and most dark matter-dominated (Simon & Geha 2007) galaxies known. Their average metallicities are less than typical globular clusters (Kirby et al. 2008). Analysis of *HST* photometry implies stellar ages at least as old as the oldest known globular clusters (Brown et al. 2012). Thus, the UFDs are a prime environment to test predicted IMF variations with the temperature, den-

[1] Based on observations made with the NASA/ESA *Hubble Space Telescope*, obtained at STScI, which is operated by AURA, Inc., under NASA contract NAS 5-26555.

[2] Astronomy Department, Yale University, New Haven, CT 06520, USA; marla.geha@yale.edu
[3] Space Telescope Science Institute, 3700 San Martin Drive, Baltimore, MD 21218, USA; tbrown@stsci.edu, tumlinson@stsci.edu
[4] University of Physics & Astronomy, University of California Irvine, 4129 Frederick Reines Hall, Irvine, CA 92697, USA
[5] Center for Galaxy Evolution Fellow
[6] Department of Physics and Astronomy, University of Victoria, P.O. Box 3055, Victoria, BC, V8W 3P6, Canada
[7] Departamento de Astronomía, Universidad de Chile, Casilla 36-D, Santiago, Chile
[8] Observatories of the Carnegie Institution of Washington, 813 Santa Barbara Street, Pasadena, CA 91101, USA
[9] UCO/Lick Observatory and Department of Astronomy and Astrophysics, University of California, Santa Cruz, CA 95064, USA

sity, or cosmic epoch of the star-forming environment (Tumlinson 2007).

Direct estimates of the IMF based on counting resolved main-sequence stars are largely limited to the nearby Galactic field and star clusters (Bastian et al. 2010). Milky Way open clusters provide a relatively large stellar mass range over which to measure the IMF (0.08 – 7 $M_\odot$, e.g., Moraux et al. 2004), but are more metal-rich than the UFDs. At metallicities less than [Fe/H] < -1, *HST* studies of Galactic globular clusters probe the IMF down to main sequence masses between $0.2 - 0.7\,M_\odot$ (Paust et al. 2010). However, dynamical evolution, such as mass segregation and evaporation, can significantly change the slope of the mass function (Vesperini & Heggie 1997; Baumgardt & Makino 2003). Interestingly, the observed MF slopes correlate contrary to expectation with concentration (De Marchi et al. 2010). The observed correlation can be understood as dynamical evolution combined with either gas expulsion of residual gas (Marks et al. 2012), or related to orbital properties and the degree of tidal stripping (Küpper et al. in prep.).

Dwarf galaxies have metallicities similar to or lower than Galactic globular clusters, but have relaxation times longer than a Hubble time and therefore do not require corrections for dynamical evolution. Dwarf galaxies in which the low mass IMF has been directly measured are the Milky Way satellites Ursa Minor ($M_V = -9.2$, [Fe/H] $= -2.0$), Draco ($M_V = -8.6$, [Fe/H] $= -2.0$), and the Small Magellanic Cloud (SMC; $M_V = -15$; [Fe/H] $= -1.2$). Wyse et al. (2002) used *HST*/WFPC2 data to conclude that the Ursa Minor IMF is consistent with a power law slope $\alpha = 1.8$ over the mass range $0.4 - 0.7\ M_\odot$. Grillmair et al. (1998) found a power law slope for the Draco dwarf galaxy between $2.1 < \alpha < 2.3$ for an assumed age of 12 Gyr, based on *HST*/WFPC2 imaging extending to $0.6\,M_\odot$. Kalirai et al. (2013) used *HST*/ACS data to conclude that the IMF of the SMC has a power law slope of $\alpha = 1.90^{+0.10}_{-0.15}$ over the mass range $0.37 - 0.93\ M_\odot$.

Using the *HST*/ACS we are undertaking a deep imaging survey of UFDs reaching several magnitudes below the main-sequence turnoff. The program includes the Milky Way satellites Hercules, Leo IV, Ursa Major I, Boötes I, Coma Berenices, and Canes Venatici II. In Brown et al. (2012), we presented a preliminary analysis of the stellar populations in the first three galaxies for which data had been taken. We concluded that all stars in these galaxies were older than 11 Gyr and that star formation lasted less than 2 Gyr.

Here we present a companion analysis of the IMFs for Leo IV and Hercules. Although Ursa Major I was included in the age analysis of Brown et al. (2012), the ACS catalog of this galaxy has significantly fewer stars, and these stars were observed over a much wider area (specifically, 9 ACS tiles in Ursa Major I, compared to 1 and 2 tiles in Leo IV and Hercules, respectively). While Ursa Major I is closer than either Leo IV or Hercules, it is subject to significant contamination from image artifacts and field contamination, and does not provide a good constraint on the IMF. We therefore do not include Ursa Major I in our analysis.

In § 2 we describe the *HST*/ACS data and construction of the IMFs. In § 3, we use these data to constrain the IMF slope and binary fraction over the stellar mass range $0.52 - 0.77\,M_\odot$. In § 4, we discuss implications of our IMFs for the UFDs. In § 5, we compare these results to other direct IMF measurements and discuss them in a broader cosmological context.

TABLE 1
UFD Galaxy Properties and IMF Results

Row	Quantity	Units	Hercules	Leo IV
(1)	α (J2000)	h : m : s	16:31:05	11:32:57
(2)	δ (J2000)	° : ′ : ″	+12:47:18	−00:31:00
(3)	(m-M)$_V$	mag	20.90	21.15
(4)	Distance	kpc	135	156
(5)	E(B-V)	mag	0.08	0.06
(6)	M_V	mag	-6.2 ± 0.4	-5.5 ± 0.3
(7)	L_V	$L_\odot$	$2.6^{+1.2}_{-0.8} \times 10^4$	$1.4^{-0.4}_{-0.3} \times 10^4$
(8)	$r_{\rm eff}$	pc	230	130
(9)	σ	km s^{-1}	5.1 ± 0.9	3.3 ± 1.7
(10)	$\langle$[Fe/H]$\rangle$	dex	−2.41	−2.54
(11)	$t_{\rm relax}$	years	3×10^{12}	2×10^{12}
IMF Results				
(12)	Mass range	$M_\odot$	0.52 - 0.76	0.54 - 0.77
(13)	$N_{\rm star}$		2350	1054
(14)	α		$1.2^{+0.4}_{-0.5}$	1.3 ± 0.8
(15)	m_c	$M_\odot$	$0.4^{+0.9}_{-0.3}$	$0.4^{+2.1}_{-0.3}$
(16)	$f_{\rm binary}$		$0.48^{+0.20}_{-0.12}$	$0.47^{+0.37}_{-0.17}$

Note. — (1-2) Right ascension and declination taken from Martin et al. (2008). (3-5) The distance modulus, distance and reddening are best fitting values from the *HST* CMDs. (5-7) Absolute magnitudes and effective radii from Sand et al. (2009) and Sand et al. (2010) for Hercules and Leo IV, respectively. (7-8) Velocity dispersion and average metallicity from Simon & Geha (2007) and Kirby et al. (2011). (9) The two-body relaxation is calculated using the quantities in (5-7) and Equation 1.38 in Binney & Tremaine (2008). (10) Stellar mass range (10) and number of stars (11) included in our IMF analysis. (11-13) Estimated IMF parameters in the mass range $0.52 - 0.77\,M_\odot$. Binary fractions (14) are given for the power law fits.

2. OBSERVATIONS AND DATA REDUCTION

The Hercules and Leo IV UFDs were discovered by Belokurov et al. (2007) as statistically significant overdensities of stars in the SDSS. As listed in Table 1, Hercules and Leo IV have average metallicities of $\langle$[Fe/H]$\rangle$ $= -2.4$ and -2.5, respectively, and show internal metallicity spreads of more than 0.5 dex (Kirby et al. 2008; Adén et al. 2009). Both galaxies contain a population of RR Lyrae stars, implying the presence of stars that are at least as old as 10 Gyr (Moretti et al. 2009; Musella et al. 2012). Ground-based imaging further suggested old stellar populations (Coleman et al. 2007; Sand et al. 2010; de Jong et al. 2010; Okamoto et al. 2012). Coleman et al. (2007) and Deason et al. (2012) suggest that Hercules is tidally disrupting due to its elongated shape and velocity gradient at large radius. Since tidal processes are independent of stellar mass this should not affect the IMF analysis, and our *HST* observations described below are well within the gravitationally bound region of the object. Based on the same *HST* observations described below, Brown et al. (2012) confirmed that stars in these two UFDs are exclusively 11 Gyr or older.

We obtained deep optical images for Hercules and Leo IV using the F606W and F814W filters on the *HST*/ACS Wide Field Camera between August 2011 and January 2012 (GO-12549, PI: Brown). The total exposure times were 25625 and 41060 seconds, respectively. We obtained two ACS tiles for Hercules and one ACS tile

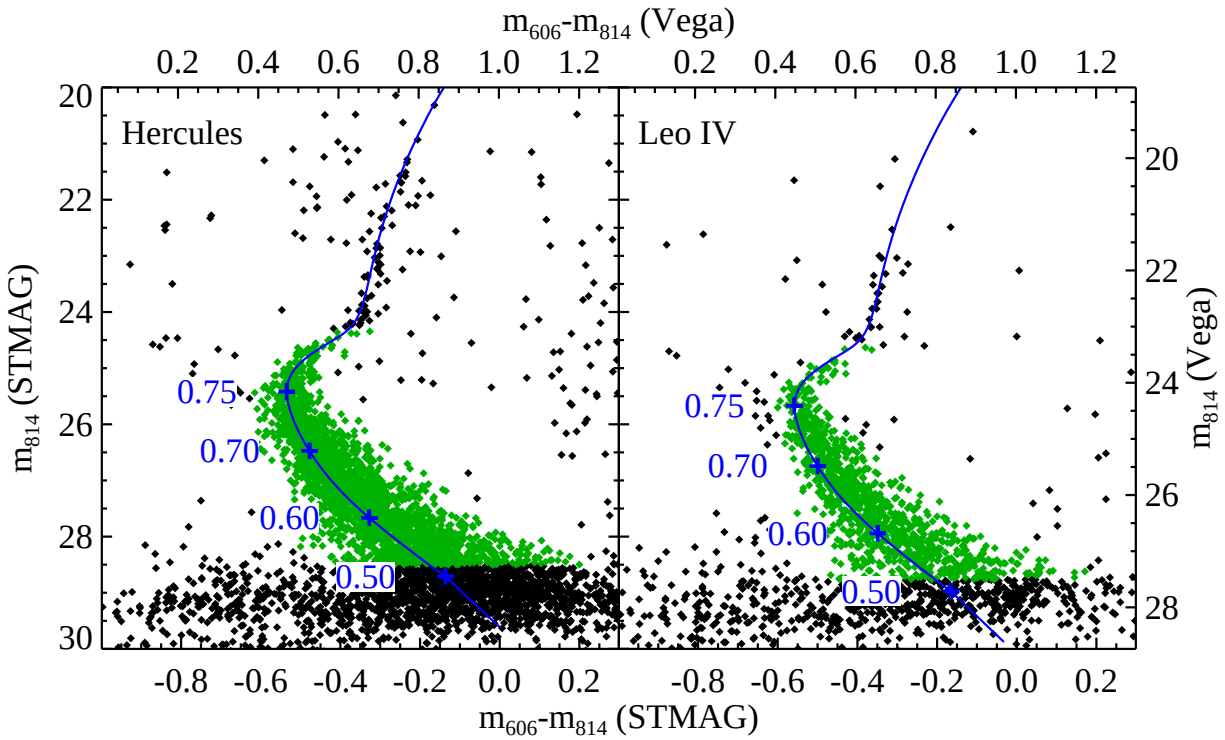

FIG. 1.— The *HST*/ACS CMDs of two UFD galaxies, Hercules (*left*) and Leo IV (*right*). For the IMF analysis, we include stars below the sub-giant branch and above the 66% and 75% completeness limits for Hercules and Leo IV, respectively (green points). The axes are labeled in both STMAG and Vega magnitudes. The blue line is a representative isochrone of 13.6 Gyr and the mean metallicity of each galaxy (Table 1). Blue crosses indicate stellar mass in units of $M_{\odot}$ on the main sequence.

for Leo IV. All images were dithered to mitigate detector artifacts and enable resampling of the point spread function (PSF). Our image processing includes the latest pixel-based correction for charge-transfer inefficiency (Anderson & Bedin 2010). We co-added the images for each filter in a given tile using the IRAF DRIZZLE package (Fruchter & Hook 2002), with masks for cosmic rays and hot pixels derived from each image stack, resulting in geometrically-correct images with a plate scale of $0.03''$ pixel^{-1} and an area of approximately $210'' \times 220''$.

We performed both aperture and PSF-fitting photometry using the DAOPHOT-II package (Stetson 1987), assuming a spatially-variable PSF constructed from isolated stars. The final catalog combined aperture photometry for bright stars with photometric errors < 0.02 mag and PSF-fitting photometry for the rest, all normalized to an infinite aperture. Due to the scarcity of bright stars, the uncertainty in the normalization is 0.02 mag. Our photometry is in the STMAG system: $m_{\lambda} = -2.5\times \log_{10} f_{\lambda} - 21.1$, except where we explicitly state Vega magnitudes (Figure 1). The catalogs were cleaned of stars with poor photometry and background galaxies. Sources were rejected based on photometric errors (< 0.1 mag) and the DAOPHOT χ and *sharp* parameters. We also reject stars with bright neighbors and those falling within the profiles of extended background galaxies because these are noisier than isolated stars of comparable magnitude. We apply the same rejection criteria in determining the completeness of our data described below. For more details on the data reduction see Brown et al. (2009).

We performed extensive artificial star tests to evaluate the photometric scatter and completeness for each galaxy. These tests employed the same PSF model and PSF-fitting routines used in the construction of the observed catalogs, including the algorithms for culling poor-quality stars, image artifacts and corrections for charge transfer efficiency. Artificial stars were inserted into the image with appropriate reductions in signal (and noise) due to charge transfer inefficiency. Stars were then blindly recovered and corrected for charge transfer (Anderson & Bedin 2010). The artificial stars were inserted over a wide range of color ($-1.3 \leq m_{606} - m_{814} \leq 0.5$) and magnitude ($32 \geq m_{814} \geq 16$) with most of the stars falling near the observed stellar locus and biased toward fainter magnitudes, thus providing the most fidelity in the analysis region. A total of 5,000,000 artificial stars were inserted into each image, spread over thousands of passes in order to avoid significantly altering the level of crowding and the associated photometric scatter. The number of stars recovered from all passes sets the completeness fractions given in Table 2. For this analysis, we include stars fainter than the red giant branch and brighter than the magnitude where photometric errors approach the main-sequence width and photometric artifacts begin to contribute significantly to the catalog (green region in Figure 1, see Table 2). The faint cutoff corresponds to the 66% and 75% completeness limits for Hercules and Leo IV, respectively. This magnitude region corresponds to a stellar mass range of $0.52-0.77\,M_{\odot}$ and includes 2380 stars in Hercules and 1054 stars in Leo IV.

2.1. *Constructing the Model IMFs*

We analyze our observed luminosity functions by forward modeling stellar evolutionary tracks with an ana-

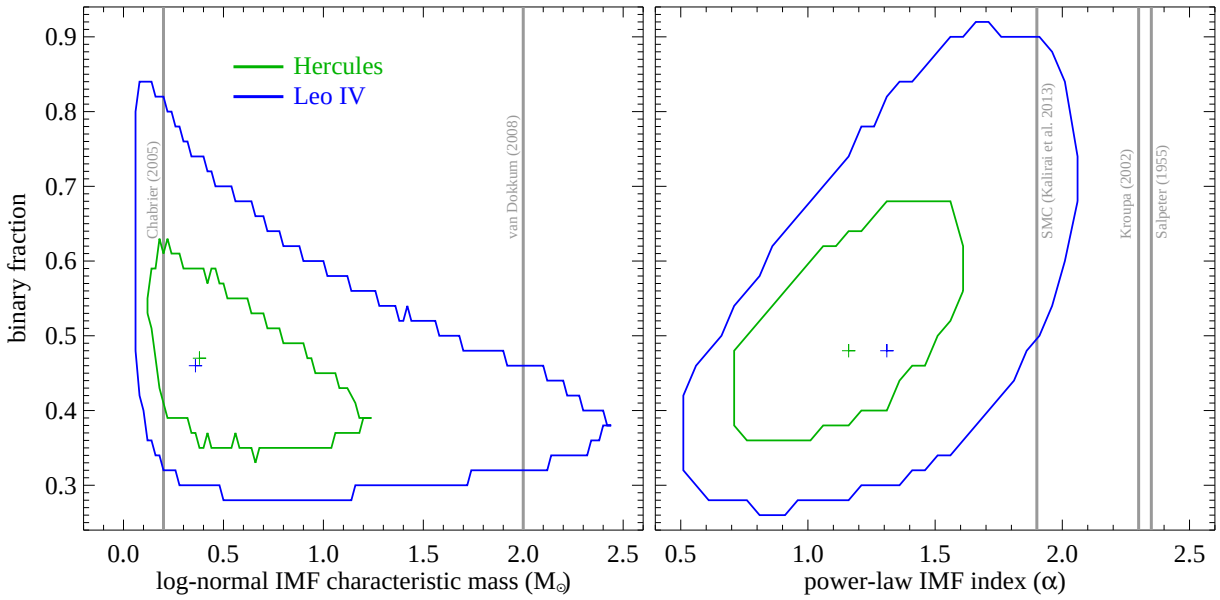

FIG. 2.— One-sigma confidence contours for the Hercules (green) and Leo IV (blue) UFD galaxies. For the mass range probed by our data ($0.52 - 0.77\,M_\odot$), we plot our results for a log-normal IMF (*left*) and power-law IMF (*right*). The best fitting combination of characteristic mass (m_c) or slope (α) and stellar binary fraction ($f_{\rm binary}$) are shown as plus symbols. For reference, we indicate values of m_c and α for IMFs in the literature.

lytic form of the IMF and our observational errors. The free parameters in our models are the IMF shape and the binary fraction. We also allow the distance and reddening of each UFD galaxy to float within the one-sigma errors of the values determined in Brown et al. (2012). Because our IMF fits exclude stars brighter than the subgiant branch, the resulting values of $(m-M)_V$ and E(B-V) are slightly different than Brown et al. (2012) at the hundredth of a magnitude level, providing a better fit to the main-sequence region. These values are listed in Table 1. We fix the galactic age to 13.6 Gyr, as determined in Brown et al. (2012). We further fix the distribution of metallicities in each UFD galaxy based on the spectroscopic metallicity distribution functions determined by Kirby et al. (2008) and Kirby et al. (2011). We explore these assumptions further below.

We simulate the observations beginning with new Victoria-Regina evolutionary tracks (VandenBerg et al., in prep.) which assume a solar heavy-element mixture by Asplund et al. (2009), with 0.4 dex enhancements in the α-element abundances, and then scaled to the [Fe/H] values of interest. These are computed using the same code described in VandenBerg et al. (2012). These isochrones are transformed into the observed STMAG magnitude system using the MARCS model atmosphere library and the throughput curves for the ACS F606W and F814W filters. The transformation is calibrated to observations of globular clusters in the same filters, with 1% agreement over the main sequence, subgiant branch, and RGB.

We assume two different functional forms of the IMF: a single power-law with free parameter α (where a Salpeter IMF is $\alpha = 2.35$, see Introduction for the functional form), and a log-normal model with parameters σ and characteristic mass m_c (where a Chabrier IMF for single stars is $\sigma = 0.69$ and $m_c = 0.2\,M_\odot$). In the case of the log-normal IMF, our stellar mass range is too small to determine the distribution width and, for the purpose of this paper, we keep this value fixed at the Chabrier value of $\sigma = 0.69$. We note that for the Milky Way IMF, current data cannot significantly differentiate between these two function forms (Kroupa et al. 2011).

The shape of the IMF is somewhat degenerate with the presence of unresolved binary stars (Kroupa et al. 1991). We have therefore opted to fit both the IMF shape and the binary fraction simultaneously. We define the binary fraction, $f_{\rm binary}$, as the fraction of unresolved systems which are binary (e.g., if 25 out of 100 systems are binary, then $f_{\rm binary} = 0.25$ and the total number of individual stars is 125). We draw binary companions from the full distribution of stellar masses, meaning that the mass ratio distribution is flat. Because we are explicitly fitting for binary fractions, the reported IMF parameters below pertain to the single-star IMF, rather than the system IMF.

We convolve the IMF with our known observational errors and completeness estimates, resulting in a stellar probability distribution for a single age and metallicity. While the UFDs likely had a period of star formation which lasted at least 100 Myr and at most 2 Gyr (Vargas et al. 2013; Brown et al. 2012), our assumption of a single age has insignificant effects on the IMF, because nearly all of the weight in our fit comes from stars below the main-sequence turnoff of the oldest population which change by less than 0.01 mag over this time period. For the fixed single age of each UFD, we linearly combine tracks for different metallicities to recreate the spectroscopic metallicity distribution function (MDF) as determined by Kirby et al. (2011) based on Keck/DEIMOS data from Simon & Geha (2007). The UFDs have significant internal metallicity dispersion, over 0.6 and 0.7 dex for Hercules and Leo IV, respectively. Since the MDFs used in this analysis are based on fewer than 25 stars in each galaxy, we roughly estimate the IMF error which may be introduced by metallicity errors. We simulate two CMDs based on our observational errors and completeness values, assuming a Salpeter IMF. For one sim-

ulated dataset, we use the observed Hercules MDF. For the second dataset, we assume a single metallicity of [Fe/H]$= -2.4$. We then recover the IMFs assuming the same single metallicity isochrone. The IMF slopes for these two simulations are less than 0.1 different in the power law slope which is far less than the 1-σ error on this parameter determined below.

The final comparison between model and observations is done in CMD space by binning each into Hess diagrams. The Hess diagrams have axes of magnitude and color with 0.1 mag bins in each axis. The model and observed Hess diagrams are then compared using the Maximum Likelihood statistic of Dolphin (2002), using the stars defined as members of each galaxy (Figure 1). We search a grid over two free parameters: the IMF slope (α for a power-law IMF) or characteristic mass (m_c for a log-normal IMF) and the binary fraction $f_{\rm binary}$. The best-fit model is that with the minimum Maximum Likelihood statistic over the two free parameters (Figure 3).

We do not correct our inferred IMFs for dynamical evolution. Dynamical two-body relaxation processes, such as mass segregation and evaporation, are mass dependent and will alter the initial stellar mass function over a relaxation timescale, which we calculate according to Equation 1.38 in Binney & Tremaine (2008): $t_{\rm relax} \sim (N/log_{10}N) * (R/\sigma)$. We assume the values for the radius (R) and stellar velocity dispersion (σ) using the values listed in Table 1. The resulting timescales are on the order of 10^{12} years, a few hundred times the age of the Universe. Thus, two-body relaxation processes can safely be ignored in the UFD galaxies.

3. RESULTS

The *HST*/ACS imaging for Hercules and Leo IV extends roughly three magnitudes below the main-sequence turnoff (Figure 1). Stars included in the IMF analysis correspond to stellar masses between $0.52 - 0.77\,M_\odot$. While this is not a particularly large range in stellar mass, it is sufficient to distinguish between various IMFs suggested in the literature.

3.1. *Constraints on the IMF*

In Figure 2, we plot the one-sigma error contours for the binary fraction and IMF parameter α or m_c, in the case of the power-law and log-normal IMF, respectively. The constraints for Hercules (green) are tighter as compared to Leo IV (blue) since Hercules is intrinsically more luminous and the ACS photometric catalog is better populated along the main sequence. The best-fit solutions are consistent between the two galaxies. Based on the maximum likelihood statistic, the power law and log-normal models provide an equally good fit to the data: the log-normal form is slightly preferred but at low (0.3σ) significance.

For a single power law model, we find a best fit slope of $\alpha = 1.2^{+0.4}_{-0.5}$ for Hercules and $\alpha = 1.3 \pm 0.8$ for Leo IV (Figure 2, right panel). In Figure 3, we plot the observed luminosity functions for each UFD and overplot our best-fitting model (green) compared to a Salpeter IMF ($\alpha = 2.35$, blue) and an extremely bottom-light IMF ($\alpha = 0.5$, red). For Hercules, the IMF slope is shallower than the Salpeter ($\alpha = 2.35$) and Kroupa ($\alpha = 2.3$ above $0.5\,M_\odot$) IMF at the 5.8-σ and 5.4-σ levels. For Leo IV, the Salpeter and Kroupa values are 1.9-σ and 1.7σ from our best fit value. We note that our error contours are non-Gaussian. While we strongly rule out the Salpeter and Kroupa values for Hercules, we note that just below our mass range of $0.52 - 0.77\,M_\odot$ the Milky Way IMF slope turns over. Below $0.5\,M_\odot$, the Kroupa IMF slope changes to $\alpha = 1.3$, which is well within the UFD values. The exact location of this turn over in the Milky Way is unclear. For example the data from Bochanski et al. (2010) plotted in Figure 4 suggests a Salpeter-like slope down to $0.3\,M_\odot$. We will discuss this further in § 5. Our power-law slopes are also shallower than recent IMF results in the Small Magellanic Cloud. Kalirai et al. (2013) found $\alpha = 1.90^{+0.10}_{-0.15}$ over the mass range $m = 0.37 - 0.93\ M_\odot$, which is 2.3-σ away from the Hercules IMF. These authors also fit a power law only to stars more massive than $0.6\,M_\odot$, finding a slope $\alpha = 2.1 \pm 0.3$.

We alternatively fit a log-normal function to our UFD data, showing the one-sigma confidence intervals in the left panel of Figure 2. The best-fitting log-normal IMF values are: $m_c = 0.4^{+0.9}_{-0.3}\,M_\odot$ for Hercules and $m_c = 0.4^{+2.1}_{-0.3}\,M_\odot$ for Leo IV. The Milky Way value of $m_c = 0.2\ M_\odot$ (Chabrier 2005) is within our 1-σ errors. However, the fact that the data prefer a more massive characteristic mass is consistent with the results for our power law fits, since, in our mass range, a more massive characteristic mass provides an overall flatter IMF shape as determined for the power law slope. In addition, the data for Hercules rule out an extremely 'bottom-light' IMF, with $m_c \sim 2\,M_\odot$, as favored by van Dokkum (2008) for massive elliptical galaxies, although this result has been subsequently disputed (van Dokkum & Conroy 2011).

In Figure 4, we plot the mass function of our UFDs. We compute the mass function by converting the completeness corrected F814W luminosity function (Table 2) into stellar mass assuming the best fitting single Victoria-Regina isochrone and rebinning using constant logarithmic mass bins. While this method does not fully take into account metallicity spread or photometric errors (which are accounted for in our formal analysis, § 2.1), this effect is small and allows us to compare more directly to literature data. Published luminosity functions are available for two other galaxies with low mass IMF analyses. We convert the luminosity functions for the SMC (Table 1 in Kalirai et al. 2012) and the dwarf spheroidal galaxy Ursa Minor (Table 9 in Wyse et al. 2002) into mass functions in the same manner as the UFDs based on the best-fitting single isochrone. Literature data for the mass function itself is available only for the Milky Way and we plot data from Table 11 in Bochanski et al. (2010) based on SDSS photometry of Milky Way field stars. We have arbitrarily renormalized the mass functions and overplot representative analytic fits. While Figure 4 emphasizes the limited stellar range over which the UFD IMFs have been measured, it visually confirms that the UFD IMF slopes are shallower than the observed Milky Way and SMC IMFs. We explore the implications of a shallow IMF for the UFDs in § 4 and discuss these results in the context of other galaxies in § 5

3.2. *Constraints on the Binary Fractions*

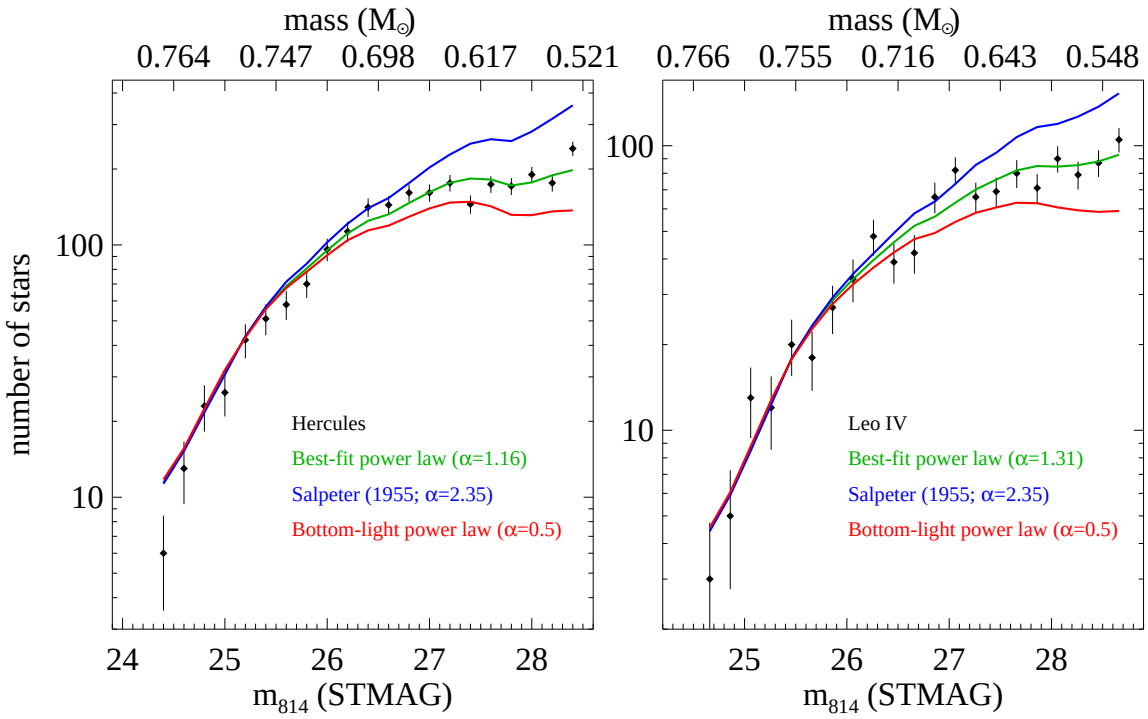

FIG. 3.— The observed luminosity function for Hercules (*left*) and Leo IV (*right*). Errors bars are computed from the observed number of stars in each luminosity bin. For comparison, we plot three theoretical power law IMFs, convolved with our observational errors and photometric completeness. The fits were normalized to reproduce the number of stars in the observed luminosity function, but here they have been normalized at the bright end for clarity. We compare our best-fitting model (green) to a Salpeter IMF ($\alpha = 2.35$, blue) and an extremely bottom-light IMF ($\alpha = 0.5$, red).

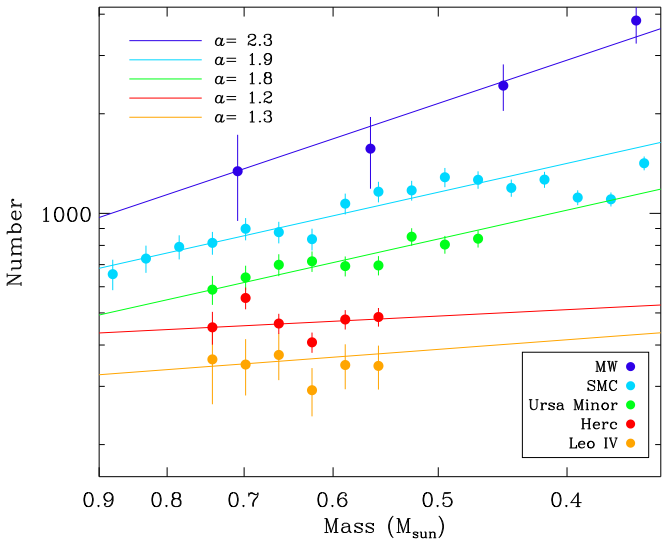

FIG. 4.— Stellar mass functions for the five galaxies in which the IMF has been measured via direct star counts: the Milky Way (blue, Bochanski et al. 2010), the SMC (light blue, Kalirai et al. 2012), Ursa Minor dSph (green; Wyse et al. 2002), Leo IV (orange; this work) and Hercules (red; this work). Except for Hercules, the vertical normalization is arbitrary. For reference, the published power law slopes are shown for each dataset, normalized at $0.75\,M_\odot$. We note that a power law slope of $\alpha = 1$ is a flat line in this log-log plot. The UFD galaxies show noticeably flatter mass functions in this mass range.

The presence of unresolved binary stars can mimic a flattening of the IMF at low masses (Kroupa et al. 1991; Bochanski et al. 2010). On the main sequence, Kroupa et al. (1991) first demonstrated that unresolved binary systems widen the main sequence beyond observational errors, with binary systems brighter and redward of the single star main sequence. Our best-fitting single-power law IMF is degenerate between steeper IMF slopes with high binary fractions and shallower (more bottom-light) IMF slopes with lower binary fractions (Figure 2). For Hercules, the binary fraction is constrained to be $f_{\rm binary} = 0.48^{+0.20}_{-0.12}$ for a single power law or $0.47^{+0.16}_{-0.14}$ for a log-normal IMF. The binary fractions for Leo IV are similar, but far less constrained due to the smaller number of observed stars (Table 1). While binary stars were known to exist in the UFDs based on repeated spectroscopic measurements of red giant branch stars (Simon et al. 2011; Koposov et al. 2011), these observations did not strongly constrain the binary fraction itself (Martinez et al. 2011). Our results are the first quantitative constraints on the binary fraction in the UFDs.

The binary fractions inferred for the UFDs pertain to stars in the mass range $0.52 - 0.77\,M_\odot$, predominantly K-dwarf stars. In the solar neighborhood, the multiplicity of stars decreases with decreasing stellar mass (Kraus & Hillenbrand 2012), with more massive OB-type stars having binary fractions upwards of $f_{\rm binary} = 0.7$ (Peter et al. 2012), down to M-stars with binary fractions between 0.2-0.3 (Janson et al. 2012). This trend may be the result of intrinsic differences in the binary fraction as a function of stellar mass, the consequence of a single overall binary fraction and random pairings across the mass spectrum, or possibly due to binary disruption over time combined with ages differences between spectral populations (Kroupa et al. 1993; Marks & Kroupa 2011). For K-dwarfs, Duquennoy & Mayor (1991) sug-

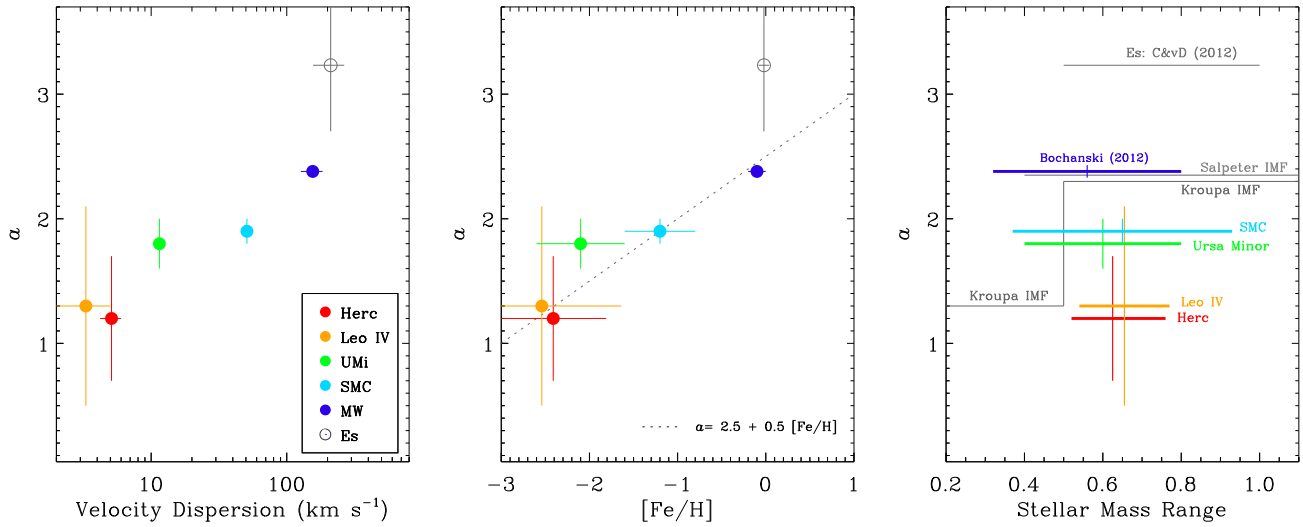

FIG. 5.— The power law slope, α, plotted against galaxy velocity dispersion (*left*), metallicity [Fe/H] (*middle*) and the observed stellar mass range (*right*). Data are taken from the same sources as Figure 4. The dotted line in the middle panel is an empirical relationship suggested by Kroupa (2001) with a zero-point shift to fit these data. Indirect measurements are shown for elliptical galaxies from Conroy & van Dokkum (2012). A trend is seen in the sense of shallower, more bottom-light IMF slopes towards less massive and more metal-poor galaxies.

gest that roughly half of solar neighborhood K-dwarf systems are binary; a recent analysis by Raghavan et al. (2010) find a solar neighborhood binary fraction for FGK stars of 0.46 ± 0.02. This is in remarkable agreement with our UFD binary fractions, despite the significantly lower metallicity environment of the UFDs as compared to the solar neighborhood. While noting that binary fractions as high as $f_{\rm binary} = 0.68$ are allowed within our $1-\sigma$ limits for Hercules, the best-fitting binary fractions appear to be a more 'universal' property than the slope of the IMF (Marks & Kroupa 2011).

4. IMPLICATIONS OF A SHALLOW IMF IN THE UFDS

The two UFDs presented have shallower IMF slopes in the stellar mass range $0.52-0.77\,M_\odot$ than expected from a Salpeter or Kroupa IMF and are marginally shallower than a Chabrier IMF over the observed mass range. This difference is seen visually in Figure 3. For an IMF slope $\alpha = 2.3$, we would have expected to observe 2900 stars as compared to the 2380 stars observed for Hercules with an inferred IMF slope of $\alpha = 1.2$. Many properties of the UFDs have been calculated assuming a standard IMF. Our results have implications for the stellar mass, mass-to-light ratio supernova rates and formation models of these low luminosity systems.

Martin et al. (2008) calculated the stellar mass of Hercules and Leo IV assuming both a Kroupa and Salpeter IMF. Since the Kroupa IMF has a shallower IMF slope below $0.5\,M_\odot$, the resulting total stellar masses are 50% that of a Salpeter IMF. If we instead use our IMF to determine stellar mass, assuming that a power law slope of $\alpha = 1.3$ applies over the full mass spectrum, our calculated stellar masses have 40% the mass of a Salpeter IMF. Alternatively, the best-fit log-normal fit with $m_c = 0.4\,M_\odot$ has 44% the stellar mass as a Chabrier IMF with $m_c = 0.2\,M_\odot$.

Shallower IMF slopes have implications for models of UFD galaxy formation. An IMF is assumed in calculating the amount of available supernova energy which is an important physical process in many galaxy formation models (e.g., Governato et al. 2012; Wyithe & Loeb 2013; Teyssier et al. 2013), particularly for dwarf galaxies. The magnitude of this effect depends in large part on the behavior of the IMF outside our observation window. If the shallow slope measured at low masses applies across the whole mass spectrum, the number of supernovae expected per luminous star would *increase* over a Salpeter or Kroupa IMF. Assuming a Milky Way-like IMF for the UFDs under-estimates the effects of supernova feedback.

5. COMPARISONS TO OTHER IMF STUDIES

The IMF has been measured via direct star counts in the stellar mass range 0.5 to $0.8\,M_\odot$ for five distinct galaxies: the Milky Way, SMC, Ursa Minor, and the two UFDs presented here. As discussed in § 3.1, we directly compare the observed mass functions for these systems in Figure 4. We next compare the published analytic fits to the IMF, focusing for simplicity only on the power law slope (α).

In Figure 5, we plot the power-law IMF slope as a function of the galactic velocity dispersion (σ), average metallicity ([Fe/H]) and stellar mass range over which each measurement was made. The velocity dispersion and metallicity of our UFDs are given in Table 1. The SMC IMF results are taken from Kalirai et al. (2013), with the galactic velocity dispersion and metallicity from Harris & Zaritsky (2006). IMF results for the Ursa Minor dwarf galaxy are from Wyse et al. (2002), with the galactic velocity dispersion from Wolf et al. (2010) and metallicity from Kirby et al. (2011). While Wyse et al. (2002) do not provide an error bar on the IMF slope, we calculate this value by fitting a linear function to the data shown in Figure 4. For the Milky Way, we use the fitted IMF values from Bochanski et al. (2010) based on a sample of Milky Way field dwarfs spanning [Fe/H] = -0.1 to -0.6. We plot the Milky Way at a velocity dispersion of $220/\sqrt{2}$ km s^{-1}, assuming the disk is embedded in an isothermal halo (Burstein et al. 1997).

Figure 5 shows a clear trend in the IMF power law slope

as a function of galactic velocity dispersion and metallicity. The power law slope becomes increasingly shallow (bottom-light) and less Salpeter-like with decreasing galaxy mass/metallicity. This confirms the visual impression observed in Figure 4. As noted in § 3.1, Hercules is 5.4-σ different than the Kroupa IMF and 2.3-σ away from the SMC value. This is the first clear evidence for IMF variations with galactic environments based on direct star counts.

We have not included globular clusters in our comparison in Figure 5. The present-day mass functions of many globular clusters have been measured down to 0.3-0.4 $M_\odot$ and these systems are of comparable metallicity to the UFD galaxies. Paust et al. (2010) and others have measured the present day IMF of Milky Way globular clusters, suggesting that globular clusters begin with a Milky Way-like IMF and that the observed variations are related to dynamical evolution. However, this does not fully explain the observed correlations and additional mechanisms, such as gas-expulsion from initially compact clusters (Marks et al. 2012) or orbital properties (Küpper et al. 2013), are needed. Because stars clusters do not form within their own dark matter halo, it is possible that star formation of these systems is more influenced by their parent galaxy. For these reasons, we do not include star clusters in our comparisons with the UFDs.

The trends seen in Figure 5 are qualitatively consistent with results in elliptical galaxies inferred via indirect methods (i.e., based on integrated galaxy light). Correlation of IMF slope with galactic velocity dispersion has been shown via spectroscopic line widths (van Dokkum & Conroy 2011; Conroy & van Dokkum 2012; Ferreras et al. 2013), fundamental plane relations (Cappellari et al. 2012a; Dutton et al. 2012) and gravitational lensing (Treu et al. 2010). These studies suggest that the most massive ellipticals have bottom-heavy IMFs, with IMF slopes steeper than Salpeter. For example, Cappellari et al. (2012b) find a systematic trend for a sample of 260 ellipiticals with velocity dispersions between 65 - 250 km s^{-1} such that the inferred IMF is closer to Kroupa/Chabrier for low velocity dispersion ellipticals, and Salpeter or steeper at highest dispersions. In Figure 5, we include for comparison the inferred IMF slopes from Conroy & van Dokkum (2012, priv. communication) based on 35 elliptical galaxies. These authors model the IMF as a broken power-law. We plot their 'α2', the IMF slope between 0.5 - 1.0 $M_\odot$, a comparable range as our UFD observations. The plotted error bars are the sample standard deviation.

A critical question raised by Figure 5 is which physical property is responsible for the observed trends with IMF slope. While we see a clear trend of increasing (steeper) IMF slopes with both increasing galactic velocity dispersion and increasing metallicity, these two physical properties are correlated (Tremonti et al. 2004). Metallicity has often been cited as an expected driver of IMF variation, such that lower metallicity gas clouds fragment into fewer low mass protostars, and thus have a more shallow IMF. Kroupa (2001) first noted a possible correlation between the IMF slope and metallicity for Milky Way clusters and suggested an empirical relation of $\alpha = 2.3 + 0.5\,[\mathrm{Fe/H}]$. The slope of this relationship fits the trend seen in the middle panel of Figure 5 and we have adjusted the zero-point by 0.2 dex to better fit the data. For massive ellipticals, the IMF slope appears to correlate more strongly with the alpha-element abundance [Mg/Fe] than either [Fe/H] or galactic velocity dispersion (Conroy & van Dokkum 2012). Since alpha-abundances are related to supernova Type II enrichment, it is plausible that star formation rates or specific star formation density is the controlling physical parameter (Weidner & Kroupa 2005). For the UFD galaxies which have $\sim 10^4\,L_\odot$ and formed stars over a period between 100 Myr to 2 Gyr (Brown et al. 2012; Vargas et al. 2013), the star formation rates (SFR) are between $10^{-5} < \mathrm{SFR} < 10^{-4}\,M_\odot\,\mathrm{year}^{-1}$. The Milky Way has a SFR of roughly 1 $M_\odot\,\mathrm{year}^{-1}$ (Robitaille & Whitney 2010) and the most massive galaxies with the steepest inferred IMFs by Conroy & van Dokkum (2012) have inferred SFRs up to 100 $M_\odot\,\mathrm{year}^{-1}$. Determining the physical properties which control the IMF in different galaxies is a key question for future studies.

6. CONCLUSIONS

We have directly measured the IMF in two UFDs via *HST*/ACS star counts. Since the UFDs are an ancient, metal-poor and nearly single age population (Brown et al. 2012) with long two-body relaxation times, these objects provide a unique environment in which to determine the low-mass stellar IMF. We find a power law IMF slope over the stellar mass range $0.52 - 0.77\,M_\odot$ of $\alpha = 1.2^{+0.4}_{-0.5}$ for Hercules and $\alpha = 1.3 \pm 0.8$ for Leo IV, where $\alpha = 2.3$ for a Kroupa (2002) IMF in this mass regime for the Milky Way. Over our mass range, the UFDs exhibit a shallow IMF deficient in low mass stars relative to the Milky Way.

Comparing to other galaxies in which the IMF has been measured via directly counting stars, we see a trend with galactic velocity dispersion and metallicity. The power law slope becomes increasingly shallow (bottom-light) with decreasing galaxy velocity dispersion and/or metallicity. This trend is qualitatively consistent with results in elliptical galaxies inferred via indirect methods (Treu et al. 2010; van Dokkum & Conroy 2011; Cappellari et al. 2012a; Dutton et al. 2012; Conroy & van Dokkum 2012). The combined data provide clear evidence for IMF variations with galactic environment. This has significant implications for galaxy formation models which often assume a Milky Way-like IMF. A galaxy-dependent IMF affects estimates of fundamental properties such as supernova feedback rates, stellar masses and chemical abundances (e.g., Ferré-Mateu et al. 2013). A critical question for future studies is understanding the physical properties which control the IMF as a function of galactic environment.

The UFD IMFs presented here cover a relatively limited range in stellar mass. The Milky Way exhibits a transition to a shallower IMF slope just below our mass limits. Testing whether a similar transition exists in the UFDs at 0.5 $M_\odot$ or lower requires deeper *HST* imaging which can reasonably probe the IMF down to the hydrogen burning limit in the closest UFDs. Alternatively, an IMF slope transition could have existed in the UFDs at higher stellar mass than our observed range. Since stars more massive than 0.77 $M_\odot$ have long since evolved

off the main sequence, testing this is difficult, but signatures may be present in the detailed chemical abundances of individual stars (Vargas et al. 2013; Tsujimoto 2011). Both methods are needed to fully characterize the shape of the IMF and thus probe the physical conditions of star formation in these extremely old and metal-poor systems.

The details of star formation and the resulting IMF have long been predicted to depend on the physical properties of the stellar birth cloud (e.g., Larson 2005; Hennebelle & Chabrier 2008; Krumholz et al. 2011; Hopkins 2012). It is remarkable that direct evidence for IMF variations with galactic environment is only now being uncovered, and underlines the utility of the UFD galaxies for extending the baseline of physical conditions in which the IMF can be directly constrained.

We thank John Bochanski, Charlie Conroy, Kevin Covey, Pieter van Dokkum, Andreas Küpper, Richard Larson, Stella Offner, Joel Primack, Risa Wechsler and Beth Willman for productive conversations. Support for GO-12549 was provided by NASA through a grant from STScI, which is operated by AURA, Inc., under NASA contract NAS 5-26555. MG acknowledges support from NSF grant AST-0908752 and the Alfred P. Sloan Foundation. ENK acknowledges support from the Southern California Center for Galaxy Evolution and partial support from NSF grant AST-1009973. R.R.M. acknowledges support from CONICYT through project BASAL PFB-06 and from the FONDECYT project N°1120013.

REFERENCES

Adén, D., Feltzing, S., Koch, A., Wilkinson, M. I., Grebel, E. K., Lundström, I., Gilmore, G. F., Zucker, D. B., Belokurov, V., Evans, N. W., & Faria, D. 2009, A&A, 506, 1147
Anderson, J. & Bedin, L. R. 2010, PASP, 122, 1035
Asplund, M., Grevesse, N., Sauval, A. J., & Scott, P. 2009, ARA&A, 47, 481
Bastian, N., Covey, K. R., & Meyer, M. R. 2010, ARA&A, 48, 339
Bate, M. R. 2009, MNRAS, 397, 232
Baumgardt, H. & Makino, J. 2003, MNRAS, 340, 227
Belokurov, V. et al. 2007, ApJ, 654, 897
Binney, J. & Tremaine, S. 2008, Galactic Dynamics: Second Edition (Princeton University Press)
Bochanski, J. J., Hawley, S. L., Covey, K. R., West, A. A., Reid, I. N., Golimowski, D. A., & Ivezić, Ž. 2010, AJ, 139, 2679
Brown, T. M., Smith, E., Ferguson, H. C., Guhathakurta, P., Kalirai, J. S., Kimble, R. A., Renzini, A., Rich, R. M., Sweigart, A. V., & Vanden Berg, D. A. 2009, ApJS, 184, 152
Brown, T. M., Tumlinson, J., Geha, M., Kirby, E. N., VandenBerg, D. A., Muñoz, R. R., Kalirai, J. S., Simon, J. D., Avila, R. J., Guhathakurta, P., Renzini, A., & Ferguson, H. C. 2012, ApJ, 753, L21
Burstein, D., Bender, R., Faber, S., & Nolthenius, R. 1997, AJ, 114, 1365
Cappellari, M., McDermid, R. M., Alatalo, K., Blitz, L., Bois, M., Bournaud, F., Bureau, M., Crocker, A. F., Davies, R. L., Davis, T. A., de Zeeuw, P. T., Duc, P.-A., Emsellem, E., Khochfar, S., Krajnović, D., Kuntschner, H., Lablanche, P.-Y., Morganti, R., Naab, T., Oosterloo, T., Sarzi, M., Scott, N., Serra, P., Weijmans, A.-M., & Young, L. M. 2012a, Nature, 484, 485
Cappellari, M., McDermid, R. M., Alatalo, K., Blitz, L., Bois, M., Bournaud, F., Bureau, M., Crocker, A. F., Davies, R. L., Davis, T. A., de Zeeuw, P. T., Duc, P.-A., Emsellem, E., Khochfar, S., Krajnovic, D., Kuntschner, H., Morganti, R., Naab, T., Oosterloo, T., Sarzi, M., Scott, N., Serra, P., Weijmans, A.-M., & Young, L. M. 2012b, ArXiv e-prints
Chabrier, G. 2003, PASP, 115, 763
Chabrier, G. 2005, in Astrophysics and Space Science Library, Vol. 327, The Initial Mass Function 50 Years Later, ed. E. Corbelli, F. Palla, & H. Zinnecker, 41
Coleman, M. G., de Jong, J. T. A., Martin, N. F., Rix, H.-W., Sand, D. J., Bell, E. F., Pogge, R. W., Thompson, D. J., Hippelein, H., Giallongo, E., Ragazzoni, R., DiPaola, A., Farinato, J., Smareglia, R., Testa, V., Bechtold, J., Hill, J. M., Garnavich, P. M., & Green, R. F. 2007, ApJ, 668, L43
Conroy, C. & van Dokkum, P. G. 2012, ApJ, 760, 71
Covey, K. R., Hawley, S. L., Bochanski, J. J., West, A. A., Reid, I. N., Golimowski, D. A., Davenport, J. R. A., Henry, T., Uomoto, A., & Holtzman, J. A. 2008, AJ, 136, 1778
de Jong, J. T. A., Martin, N. F., Rix, H.-W., Smith, K. W., Jin, S., & Macciò, A. V. 2010, ApJ, 710, 1664
De Marchi, G., Paresce, F., & Portegies Zwart, S. 2010, ApJ, 718, 105
Deason, A. J., Belokurov, V., Evans, N. W., Watkins, L. L., & Fellhauer, M. 2012, MNRAS, 425, L101
Dolphin, A. E. 2002, MNRAS, 332, 91
Duquennoy, A. & Mayor, M. 1991, A&A, 248, 485
Dutton, A. A., Mendel, J. T., & Simard, L. 2012, MNRAS, 422, L33
Ferré-Mateu, A., Vazdekis, A., & de la Rosa, I. G. 2013, MNRAS, 431, 440
Ferreras, I., Barbera, F. L., Rosa, I. G. d. l., Vazdekis, A., Carvalho, R. R. d., Falcón-Barroso, J., & Ricciardelli, E. 2013, MNRAS, 429, L15
Fruchter, A. S. & Hook, R. N. 2002, PASP, 114, 144
Governato, F., Zolotov, A., Pontzen, A., Christensen, C., Oh, S. H., Brooks, A. M., Quinn, T., Shen, S., & Wadsley, J. 2012, MNRAS, 422, 1231
Grillmair, C. J., Mould, J. R., Holtzman, J. A., Worthey, G., Ballester, G. E., Burrows, C. J., Clarke, J. T., Crisp, D., Evans, R. W., Gallagher, III, J. S., Griffiths, R. E., Hester, J. J., Hoessel, J. G., Scowen, P. A., Stapelfeldt, K. R., Trauger, J. T., Watson, A. M., & Westphal, J. A. 1998, AJ, 115, 144
Harris, J. & Zaritsky, D. 2006, AJ, 131, 2514
Hennebelle, P. & Chabrier, G. 2008, ApJ, 684, 395
Hopkins, P. F. 2012, MNRAS, 423, 2037
Janson, M., Hormuth, F., Bergfors, C., Brandner, W., Hippler, S., Daemgen, S., Kudryavtseva, N., Schmalzl, E., Schnupp, C., & Henning, T. 2012, ApJ, 754, 44
Kalirai, J. S., Anderson, J., Dotter, A., Richer, H. B., Fahlman, G. G., Hansen, B. M. S., Hurley, J., Reid, I. N., Rich, R. M., & Shara, M. M. 2013, ApJ, 763, 110
Kirby, E. N., Lanfranchi, G. A., Simon, J. D., Cohen, J. G., & Guhathakurta, P. 2011, ApJ, 727, 78
Kirby, E. N., Simon, J. D., Geha, M., Guhathakurta, P., & Frebel, A. 2008, ApJ, 685, L43
Koposov, S. E., Gilmore, G., Walker, M. G., Belokurov, V., Wyn Evans, N., Fellhauer, M., Gieren, W., Geisler, D., Monaco, L., Norris, J. E., Okamoto, S., Peñarrubia, J., Wilkinson, M., Wyse, R. F. G., & Zucker, D. B. 2011, ApJ, 736, 146
Kraus, A. L. & Hillenbrand, L. A. 2012, ApJ, 757, 141
Kroupa, P. 2001, MNRAS, 322, 231
Kroupa, P. 2002, Science, 295, 82
Kroupa, P., Gilmore, G., & Tout, C. A. 1991, MNRAS, 251, 293
Kroupa, P., Tout, C. A., & Gilmore, G. 1993, MNRAS, 262, 545
Kroupa, P., Weidner, C., Pflamm-Altenburg, J., Thies, I., Dabringhausen, J., Marks, M., & Maschberger, T. 2011, astro-ph/1112.3340
Krumholz, M. R., Klein, R. I., & McKee, C. F. 2011, ApJ, 740, 74
Larson, R. B. 2005, MNRAS, 359, 211
Marks, M. & Kroupa, P. 2011, MNRAS, 417, 1702
Marks, M., Kroupa, P., Dabringhausen, J., & Pawlowski, M. S. 2012, MNRAS, 422, 2246
Martin, N. F., de Jong, J. T. A., & Rix, H.-W. 2008, ApJ, 684, 1075
Martinez, G. D., Minor, Q. E., Bullock, J., Kaplinghat, M., Simon, J. D., & Geha, M. 2011, ApJ, 738, 55
Moraux, E., Kroupa, P., & Bouvier, J. 2004, A&A, 426, 75

Moretti, M. I., Dall'Ora, M., Ripepi, V., Clementini, G., Di Fabrizio, L., Smith, H. A., DeLee, N., Kuehn, C., Catelan, M., Marconi, M., Musella, I., Beers, T. C., & Kinemuchi, K. 2009, ApJ, 699, L125
Muñoz, R. R., Geha, M., & Willman, B. 2010, AJ, 140, 138
Musella, I., Ripepi, V., Marconi, M., Clementini, G., Dall'Ora, M., Scowcroft, V., Moretti, M. I., Di Fabrizio, L., Greco, C., Coppola, G., Bersier, D., Catelan, M., Grado, A., Limatola, L., Smith, H. A., & Kinemuchi, K. 2012, ApJ, 756, 121
Myers, A. T., Krumholz, M. R., Klein, R. I., & McKee, C. F. 2011, ApJ, 735, 49
Okamoto, S., Arimoto, N., Yamada, Y., & Onodera, M. 2012, ApJ, 744, 96
Paust, N. E. Q., Reid, I. N., Piotto, G., Aparicio, A., Anderson, J., Sarajedini, A., Bedin, L. R., Chaboyer, B., Dotter, A., Hempel, M., Majewski, S., Marín-Franch, A., Milone, A., Rosenberg, A., & Siegel, M. 2010, AJ, 139, 476
Peter, D., Feldt, M., Henning, T., & Hormuth, F. 2012, A&A, 538, A74
Raghavan, D., McAlister, H. A., Henry, T. J., Latham, D. W., Marcy, G. W., Mason, B. D., Gies, D. R., White, R. J., & ten Brummelaar, T. A. 2010, ApJS, 190, 1
Robitaille, T. P. & Whitney, B. A. 2010, ApJ, 710, L11
Salpeter, E. E. 1955, ApJ, 121, 161
Sand, D. J., Olszewski, E. W., Willman, B., Zaritsky, D., Seth, A., Harris, J., Piatek, S., & Saha, A. 2009, ApJ, 704, 898
Sand, D. J., Seth, A., Olszewski, E. W., Willman, B., Zaritsky, D., & Kallivayalil, N. 2010, ApJ, 718, 530
Simon, J. D. & Geha, M. 2007, ApJ, 670, 313
Simon, J. D., Geha, M., Minor, Q. E., Martinez, G. D., Kirby, E. N., Bullock, J. S., Kaplinghat, M., Strigari, L. E., Willman, B., Choi, P. I., Tollerud, E. J., & Wolf, J. 2011, ApJ, 733, 46
Stetson, P. B. 1987, PASP, 99, 191
Teyssier, R., Pontzen, A., Dubois, Y., & Read, J. I. 2013, MNRAS, 493
Tremonti, C. A., Heckman, T. M., Kauffmann, G., Brinchmann, J., Charlot, S., White, S. D. M., Seibert, M., Peng, E. W., Schlegel, D. J., Uomoto, A., Fukugita, M., & Brinkmann, J. 2004, ApJ, 613, 898
Treu, T., Auger, M. W., Koopmans, L. V. E., Gavazzi, R., Marshall, P. J., & Bolton, A. S. 2010, ApJ, 709, 1195
Tsujimoto, T. 2011, ApJ, 736, 113
Tumlinson, J. 2007, ApJ, 665, 1361
van Dokkum, P. G. 2008, ApJ, 674, 29
van Dokkum, P. G. & Conroy, C. 2011, ApJ, 735, L13
VandenBerg, D. A., Bergbusch, P. A., Dotter, A., Ferguson, J. W., Michaud, G., Richer, J., & Proffitt, C. R. 2012, ApJ, 755, 15
Vargas, L. C., Geha, M., Kirby, E. N., & Simon, J. D. 2013, ApJ, 767, 134
Vesperini, E. & Heggie, D. C. 1997, MNRAS, 289, 898
Weidner, C. & Kroupa, P. 2005, ApJ, 625, 754
Willman, B. et al. 2005, ApJ, 626, L85
Wolf, J., Martinez, G. D., Bullock, J. S., Kaplinghat, M., Geha, M., Muñoz, R. R., Simon, J. D., & Avedo, F. F. 2010, MNRAS, 406, 1220
Wyithe, J. S. B. & Loeb, A. 2013, MNRAS, 428, 2741
Wyse, R. F. G., Gilmore, G., Houdashelt, M. L., Feltzing, S., Hebb, L., Gallagher, III, J. S., & Smecker-Hane, T. A. 2002, New Astronomy, 7, 395

TABLE 2
Luminosity Function for Hercules and Leo IV

F814W (STMAG)	Herc $N_{*,\mathrm{raw}}$	Herc $f_{*,\mathrm{compl}}$	Leo IV $N_{*,\mathrm{raw}}$	Leo IV $f_{*,\mathrm{compl}}$
24.35	4	0.91	.	.
24.45	2	0.90	.	.
24.55	5	0.90	.	.
24.65	8	0.90	3	0.94
24.75	15	0.90	0	0.94
24.85	8	0.90	3	0.93
24.95	8	0.90	5	0.93
25.05	18	0.89	6	0.92
25.15	20	0.89	6	0.93
25.25	22	0.88	4	0.93
25.35	25	0.88	12	0.92
25.45	26	0.88	9	0.92
25.55	32	0.87	10	0.91
25.65	26	0.86	8	0.91
25.75	34	0.86	11	0.90
25.85	36	0.86	12	0.90
25.95	40	0.85	16	0.90
26.05	56	0.85	18	0.90
26.15	63	0.83	18	0.88
26.25	50	0.83	23	0.89
26.35	70	0.83	25	0.87
26.45	71	0.82	23	0.87
26.55	56	0.82	18	0.87
26.65	88	0.81	23	0.87
26.75	78	0.80	24	0.85
26.85	83	0.80	33	0.85
26.95	83	0.79	29	0.85
27.05	78	0.79	41	0.84
27.15	92	0.78	44	0.84
27.25	84	0.77	29	0.83
27.35	83	0.76	47	0.83
27.45	62	0.75	27	0.83
27.55	88	0.72	31	0.82
27.65	86	0.70	41	0.82
27.75	88	0.68	43	0.81
27.85	83	0.67	31	0.81
27.95	96	0.66	44	0.80
28.05	94	0.66	39	0.80
28.15	85	0.66	42	0.79
28.25	91	0.66	40	0.78
28.35	111	0.66	44	0.76
28.45	130	0.66	53	0.76
28.55	.	.	36	0.76
28.65	.	.	48	0.75
28.75	.	.	35	0.75

Note. — The luminosity function and photometric completeness values. We list values only for the magnitude range included in the IMF analysis.